

Use of 3D-ASL and VBM to analyze abnormal changes in brain perfusion and gray areas in nasopharyngeal carcinoma patients undergoing radiotherapy.

Fang Hu^{1,2#}, Tao Li^{2#}, Zhiqiang Wang², Shengfu Zhang³, Xiangri Wang⁴, Hong Zhou⁵, Shijun Qiu^{1,6*}

¹Department of Medical Imaging Center, Nanfang Hospital, Southern Medical University, Guangzhou, PR China

²Department of Medical Imaging, Institute of Medical Imaging and Inspection Technology, Xiangnan University, Chenzhou, PR China

³Department of Oncology, the First People Hospital of Chen Zhou, Chenzhou, PR China

⁴Department of Medical Imaging Center, the First people Hospital of Chen Zhou, Chenzhou, PR China

⁵Department of Radiology, the First Affiliated Hospital of University of South China, Hengyang, PR China

⁶Department of Medical Imaging, the First Affiliated Hospital, Guangzhou University of Traditional Chinese Medicine, Guangzhou, PR China

#These authors contributed equally to this work

Abstract

Objectives: Three-dimensional Arterial Spin Labeling (ASL) and Voxel-Based Morphometry (VBM) methods were used to demonstrate whole-brain perfusion and gray matter volume abnormalities after Radiotherapy (RT) for Nasopharyngeal Carcinoma (NPC).

Methods: Fifty participants with NPC were divided into Pre-RT Control (PC), Acute Reaction Period (ARP), and Delayed Reaction Period (DRP) groups based on the course of RT. A Region of Interest (ROI) based analysis was performed on the Cerebral Blood Flow (CBF) and anatomic data.

Results: Compared with the PC group, increased perfusion in the left cerebellum, left paracentral lobule, and bilateral thalamus was noted in the ARP group ($p < 0.05$), while patients in the DRP group showed no significant differences when compared to the other two groups ($p > 0.05$). The relative Gray Matter Volume (rGMV) was decreased in the right paracentral lobule in the ARP group, but increased in the bilateral cerebellum in the DRP group compared to the PC group, and increased in the left cerebellum, bilateral cerebellum and right paracentral lobule in the ARP group as well (all $p < 0.05$). Moreover, the CBF was negatively correlated with the rGMV in several specific brain areas ($p < 0.05$).

Conclusion: ASL facilitated non-invasive detection of radiation-induced whole-brain gray matter perfusion changes, which were transient, dynamic, complicated, and negatively correlated with the GMV.

Keywords: Nasopharyngeal carcinoma (NPC), Radiation therapy (RT), Cerebral blood flow (CBF), Three-dimensional arterial spin labelling (ASL), Voxel-based morphometry (VBM).

Accepted on August 21, 2017

Introduction

Radiotherapy (RT) plays an indispensable role in the curative treatment for patients with Nasopharyngeal Carcinoma (NPC). However, the brain tissue is quite vulnerable to radiation, which is inevitably contained within the radiation field. Therefore, acute and late effects of RT on the brain tissue are frequent [1]. Numerous studies have adopted special MRI methods to investigate minor changes in temporal White Matter (WM) or whole brain after RT [2-5]. However, few

studies have explored the global Cerebral Blood Flow (CBF) or Gray Matter (GM) changes. Thus, whole brain perfusion and structural alterations in NPC patients undergoing RT are unclear, as is the relationship between CBF and GM changes.

CBF is an important physiologic parameter for investigating brain perfusion and function [6]. By employing endogenous arterial blood water as a tracer, three-dimensional Arterial Spin Labeling (ASL) can provide reliable and non-invasive CBF measurements, and is thus a great choice to measure CBF in

humans [7,8]. Voxel-Based Morphometry (VBM) assesses Gray Matter Volume (GMV) voxel-by-voxel, and has been used extensively in structural investigations [9-12]. The objective of the current study was to use a new three-dimensional fast spin echo pseudo-continuous ASL (3D FSE pCASL) MRI sequence to detect perfusion distribution abnormalities in the whole brain caused by RT for NPC and explore the relationship with gray matter changes, and to supplement imaging evidence of hemodynamically-related pathophysiology for brain tissue impairment induced by RT.

Materials and Methods

This study was conducted according to the World Medical Association Declaration of Helsinki. The local Medical Ethics Committee approved the study. After the procedures of the study were explained, written informed consent was obtained from all individuals.

Subjects

A total of 50 patients pathologically-diagnosed with NPC based on biopsy were enrolled. All participants were Hans, right-handed, and divided into pre-RT control (PC (before RT)), acute reaction period (ARP (received the first RT in the past 1-6 months)), and delayed reaction period (DRP (received the first RT in 7-24 months)) groups. The exclusion criteria were as follows: -patients diagnosed with intracranial primary tumors; a history of intracranial surgery or head injury that could affect brain perfusion; left-handedness; and routine MRI abnormalities or contraindications for MRI. The routine MRI images were examined by two experienced neuro-radiologists.

Imaging protocol

A general electric 3.0 Tesla HD Signa Excite scanner with an 8-channel phased array head coil was used to obtain ASL images, structural and routing protocol images from all 56 participants. ASL images were obtained with a 3D FSE pCASL sequence (bandwidth= \pm 62.5 kHz, TR/TE=1,350/5, flip angle=155°, thickness=4 mm, post-label delay time=1,525 ms, image reconstruction matrix=128 \times 128, field of view=24 cm, and number of excitations (NEX)=3). Whole brain anatomic images were acquired using a high-resolution (1 \times 1 \times 1.2 mm voxel) reference axial 3D brain volume imaging (3D-BRAVOY™; GE Healthcare, American) sequence (TR/TE=10/7, TI=300 ms, flip angle=15°, NEX=1). A T2-weighted fluid-attenuated inversion-recovery (T2-Flair) sequence was acquired to examine brain matter abnormalities (TR/TE=5,000/72.5).

A total of 248 anatomic images, 76 ASL images scanned by MRI and 38 CBF maps automatically generated based on ASL data for each patient were acquired for further data analysis. Participants were asked to remain still with their eyes closed in the scanner.

Data analysis

One of the authors performed image pre-processing using Statistical Parametric Mapping software (SPM8; Welcome Department of Cognitive Neurology, UK <http://www.fil.ion.ucl.ac.uk/spm/>), VBM8 based on MATLAB (Math Works, Natick, MA, USA), and the Resting-state fMRI Data Analysis Toolkit (REST 1.8; <http://www.restfmri.net/forum/?q=rest13>). For each participant, ASL images were pre-processed as follows: the original image was converted to Neuroimaging Informatics Technology Initiative (NIFTI) format; the image quality was checked and individuals with low SNR were eliminated; 3D T1 image data were transformed into Montreal Neurologic Institute (MNI) space and segmented into White Matter (WM), GM, and Cerebral Spinal Fluid (CSF) and a T1 brain tissue image was created; CBF maps were accurately co-registered with the structural T1 brain images and spatially normalized into a standard stereotaxic space, and during this process, the final CBF maps were resampled to a 2 \times 2 \times 2 mm³ isotropic voxel size; CBF maps were converted into z-score maps to control individual hemodynamic variation and spatially smoothed with a 4-mm isotropic Gaussian kernel to normalize CBF maps as required and CBF values were extracted by means of anatomic Regions of Interest (ROIs), which were defined by Anatomic Automatic Labeling (AAL) templates (Figure 1).

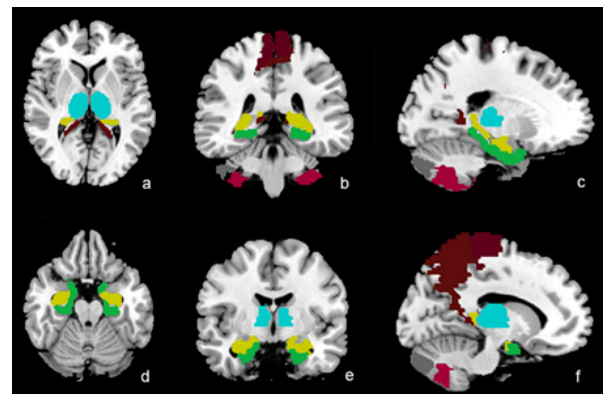


Figure 1. ROIs defined by AAL using REST. ROIs with different colors in 3 planes. Abbreviations: ROI: Region of Interest; AAL: Anatomical Automatic Labeling; REST: Resting-State fMRI Data Analysis Toolkit.

Three-dimensional structural images were processed using a toolbox for Data Processing and Analysis for Brain Imaging (Dpabi; <http://rfmri.org/dpabi14>) based on the VBM8 toolbox and Diffeomorphic Anatomical Registration Exponentiated Lie Algebra (Dartel) software. The VBM procedure involves the segmentation of the original anatomic MRI images in GM, WM, and CSF tissues, followed by GM image normalization to templates in stereotactic space to acquire optimized normalization parameters, which were applied to the raw images. Then, GM images were smoothed using a 6-mm full width at a one-half maximum (FWHM) isotropic Gaussian kernel. Finally, the relative GM volume (rGMV) was extracted by means of ROIs for further statistical analysis.

Statistical analysis

All data were represented as means ± SD (± s) of three or more independent experiments. If the data are homogenous, Analysis of variance, Student-Newman-Keulsa and Pearson’s correlation will be used. If the data are not homogenous, Kruskal-Wallis, Games-Howell test, as well as Spearman Rank Correlation analysis will be used. All the analyses were carried out using the SPSS19.0 software (SPSS Inc., Chicago, IL, USA). Values less than 0.05 were considered to be statistically significant.

Results

Demographics

Table 1 shows that all groups were essentially of equal mean age, and had a similar distribution of gender and education level (all p>0.05).

Whole-brain GM perfusion difference

When compared with the PC group, patients in the ARP group had higher perfusion in the left cerebellum_8, left cerebellum_crus_2, left paracentral lobule, and bilateral thalamus (all p<0.05). However, the DRP group had no significant statistically difference with other groups (all p>0.05), as shown in Table 2.

Gray matter volume difference

As show in Table 3, the rGMV of patients in the ARP group decreased more than the PC group in the right paracentral

lobule, and increased in the DRP group in the bilateral cerebellum_crus_2 (all p<0.05). In addition, when compared with the ARP group, the VBM showed that the GM was expanded in the DRP group in the left cerebellum_8, bilateral cerebellum_crus_2, and right paracentral lobule (all p<0.05).

Correlation between the CBF and GMV

As shown in Table 4, the whole brain GM, left cerebellum_8, right cerebellum_8, left cerebellum_crus_2, left hippocampus, right hippocampus, left parahippocampus, right precuneus, left temporal_pole_mid, and right thalamus had negative relationships between the CBF value and rGMV (all p<0.05).

Table 1. Demographic summary of participants enrolled in the study.

N	PC	ARP	DRP	Statistic value
	20	16	14	
Age (y)	52.00 ± 14.04	51.00 ± 10.05	47.64 ± 13.09	F=0.492, P=0.615
Gender (Female/male) [§]	43952	42491	41671	χ ² =1.172, p=0.556
Education (y) [*]	7.20 ± 4.34	6.84 ± 3.42	9.36 ± 3.30	F=1.923, P=0.158

Data are presented as mean ± SD. ^{*}p>0.05 for one-way analysis of covariate. [§]p>0.05 for χ² test applied to gender. Abbreviations: PC: Pre-radiation therapy Control; ARP: Acute Reaction Period; DRP: Delayed Reaction Period.

Table 2. CBF differences among the three groups.

Region name	CBF			Statistic value (p)		
	PC	ARP	DPR	ARP-PC	DRP-PC	ARP-DRP
Left cerebellum_8 [*]	46.73 ± 12.21	57.42 ± 16.05	50.67 ± 13.68	0.027	-	-
Right cerebellum_8 [*]	45.10 ± 10.96	53.63 ± 14.90	47.51 ± 13.53	-	-	-
Left cerebellum_crus_2 [*]	48.59 ± 13.65	60.48 ± 15.38	51.30 ± 16.92	0.024	-	-
Left cerebellum_crus_2	40.96 ± 10.47	49.22 ± 13.97	42.91 ± 12.90	-	-	-
Left hippocampus [*]	47.76 ± 11.02	53.37 ± 8.65	50.96 ± 8.28	-	-	-
Right hippocampus [*]	46.06 ± 9.81	51.34 ± 9.62	49.04 ± 8.67	-	-	-
Left paracentral lobule	45.63 ± 10.00	54.07 ± 12.85	52.34 ± 12.02	0.034	-	-
Right paracentral lobule	46.81 ± 10.94	54.26 ± 13.06	50.61 ± 11.42	-	-	-
Left parahippocampus [*]	48.83 ± 10.57	53.40 ± 9.20	52.61 ± 8.92	-	-	-
Right parahippocampus	47.46 ± 9.25	52.29 ± 10.05	51.73 ± 10.06	-	-	-
Left precuneus	56.50 ± 16.76	65.55 ± 16.35	62.16 ± 15.00	-	-	-
Right precuneus [*]	51.81 ± 14.86	60.62 ± 14.12	54.68 ± 12.85	-	-	-
Left temporal_pole_mid [*]	46.05 ± 13.28	49.12 ± 9.00	48.34 ± 7.96	-	-	-
Right temporal_pole_mid	43.25 ± 10.44	47.30 ± 9.00	45.88 ± 8.22	-	-	-

Left thalamus	45.22 ± 10.92	53.96 ± 11.91	50.30 ± 13.75	0.036	-	-
Right thalamus	46.63 ± 9.78	56.16 ± 13.20	51.33 ± 13.33	0.022	-	-

rGMV are presented as mean ± SD. *p<0.05 for One-way ANOVA, followed by post hoc T-test. Abbreviations: PC: Pre-radiation therapy Control; ARP: Acute Reaction Period; DRP: Delayed Reaction Period; CBF: Cerebral Blood Flow.

Table 3. rGMV differences among the three groups.

Region name	rGMV			Statistic value (p)		
	PC	ARP	DPR	ARP-PC	DRP-PC	ARP-DRP
Left cerebellum_8*	0.331 ± 0.049	0.316 ± 0.039	0.350 ± 0.032	-	-	0.032
Right cerebellum_8*	0.354 ± 0.045	0.354 ± 0.042	0.377 ± 0.032	-	-	-
Left cerebellum_crus_2*	0.420 ± 0.048	0.425 ± 0.048	0.469 ± 0.046	-	0.006	0.015
Left cerebellum_crus_2	0.363 ± 0.047	0.361 ± 0.042	0.405 ± 0.040	-	0.007	0.009
Left hippocampus*	0.469 ± 0.047	0.454 ± 0.038	0.481 ± 0.030	-	-	-
Right hippocampus*	0.422 ± 0.038	0.415 ± 0.029	0.430 ± 0.024	-	-	-
Left paracentral lobule	0.231 ± 0.029	0.225 ± 0.035	0.229 ± 0.026	-	-	-
Right paracentral lobule	0.258 ± 0.034	0.231 ± 0.036	0.257 ± 0.032	0.02	-	0.031
Left parahippocampus*	0.509 ± 0.054	0.486 ± 0.042	0.519 ± 0.036	-	-	-
Right parahippocampus	0.525 ± 0.051	0.504 ± 0.039	0.529 ± 0.025	-	-	-
Left precuneus	0.375 ± 0.047	0.365 ± 0.044	0.382 ± 0.035	-	-	-
Right precuneus*	0.383 ± 0.044	0.377 ± 0.037	0.390 ± 0.031	-	-	-
Left temporal_pole_mid*	0.432 ± 0.069	0.410 ± 0.045	0.412 ± 0.047	-	-	-
Right temporal_pole_mid	0.376 ± 0.054	0.357 ± 0.042	0.360 ± 0.034	-	-	-
Left thalamus	0.232 ± 0.019	0.230 ± 0.028	0.244 ± 0.020	-	-	-
Right thalamus*	0.249 ± 0.019	0.245 ± 0.028	0.257 ± 0.016	-	-	-

rGMV are presented as mean ± SD. *p<0.05 for One-way ANOVA, followed by post hoc T-test. Abbreviations: PC: Pre-radiation therapy Control; ARP: Acute Reaction Period; DRP: Delayed Reaction Period; rGMV: Relative Gray Matter Volume.

Table 4. Correlative analysis of CBF and rGMV in the subjects.

Region name	Statistic value	
	R	p
Whole brain GM*	-0.348	0.007
Left cerebellum_8*	-0.328	0.01
Right cerebellum_8*	-0.273	0.028
Left cerebellum_crus_2*	-0.31	0.014
Left cerebellum_crus_2	-	-
Left hippocampus*	-0.441	0.001
Right hippocampus*	-0.548	0
Left paracentral lobule	-	-
Right paracentral lobule	-	-
Left parahippocampus*	-0.313	0.013

Right parahippocampus	-	-
Left precuneus	-	-
Right precuneus*	-0.271	0.028
Left temporal_pole_mid*	-0.237	0.049
Right temporal_pole_mid	-	-
Left thalamus	-	-
Right thalamus*	-0.325	0.011

CBF and rGMV are presented as mean ± SD. *p<0.05 for correlative analysis (age and education years as covariates). Abbreviations: PC: Pre-radiation therapy Control; ARP: Acute Reaction Period; DRP: Delayed Reaction Period; CBF: Cerebral Blood Flow; rGMV: Relative Gray Matter Volume.

Discussion

A series of studies have explored microstructural changes in brain tissues induced by RT in NPC patients using MRI

Use of 3D-ASL and VBM to analyze abnormal changes in brain perfusion and gray areas in nasopharyngeal carcinoma patients undergoing radiotherapy

methods, including Diffusion Tensor Imaging (DTI) [2-5,13-15] and proton magnetic resonance spectroscopy (1H-MRS) [5,16]. Most of the studies investigating brain tissue changes have been limited to the temporal lobe. Specifically, studies using 1H-MRS has suggested that the N-acetyl aspartate (NAA)/creatine (Cr), choline (Cho)/Cr and NAA/Cho ratios decreased during the early delayed reaction, then increased similar to pre-RT [3,16]. Another study using DTI reported that the fractional anisotropy (FA) value decreased after RT. However, the Apparent Diffusion Coefficient (ADC) value significantly increased [4] in the whole brain, and extensively in white matter after RT. The Mean Diffusion (MD) values increased were in numerous brain areas [2]. All of the above studies suggested early and dynamic micro-injuries of nerve tissue after RT in the temporal region or whole brain; however, few studies have explored whole brain CBF and gray matter volume abnormalities.

In the current study, the ASL method was utilized to assess RT-induced perfusion alterations in NPC patients. A high perfusion pattern in the ARP group was observed in the left cerebellum_8, left cerebellum_crus_2, left paracentral lobule and bilateral thalamus. The physiopathology leading to brain perfusion changes may be multifactorial, including mitochondrial disturbances, vascular abnormalities, and inflammatory factors, which widely affect the brain in the long term [17-20]. The cerebellum and thalamus are close to the target area of RT, thus we speculate that the brain gray matter showing high perfusion may be directly induced by radiation. Recent animal studies have confirmed that brain blood vessels expand by radiation during the acute period, and may be lead to hyperperfusion [1,21]. However, only the right paracentral lobule had a decreased rGMV at that point in time, which indicated that high perfusion did not result in a larger GM volume.

In the DRP group, perfusion was gradually restored to near the level of the PC group; no significant difference was observed with the other groups. When compared with the ARP group; however, VBM detected expansion of the GM in the left cerebellum_8, bilateral cerebellum_crus_2 and right paracentral lobule in the DRP group. The results further established that the increase in cerebral rGMV in the DRP group was not caused by high cerebral perfusion, but may be due to other reasons, such as enlargement or increase in nerve cell or stromal element size. This finding was verified by further correlation analysis showing that the CBF and rGMV were negatively related.

Both animal experiments and a functional imaging study confirmed that brain morphology may change to adapt to function [22]. Brain perfusion alterations may also be associated with cortical thickness abnormalities [23]. Although CBF and rGMV abnormalities were observed and showed a negative relationship in several specific areas in the current study, other studies have suggested that increased cortical thickness may involve higher brain perfusion [24]. Therefore, the mechanism of how RT influences brain perfusion and structure appears to be complicated. In functional brain

disorders, perfusion pattern changes can occur independently of anatomic changes or precede anatomic changes which were established in the current study [7].

Tools of measuring brain CBF, such as dynamic susceptibility contrast-enhanced perfusion-weighted imagine (DSC-PWI), H2O15 Positron Emission Tomography (PET) and ASL are important methods in investigating brain pathophysiology and function [25-27]. Because of non-invasive features, several important technical improvements, such as ASL, it is currently possible to easily obtain whole-brain perfusion parameters, thus becoming a good choice for disease screening and routine longitudinal tracking clinically and for research purposes [28,29]. ASL is comparable to DSE-PWI with respect to CBF, and also reveals similar brain activity patterns to PET [30,31]. Furthermore, ASL has several advantages over PET or DSC-PWI, such as avoiding potentially harmful exogenous tracers, higher spatial and temporal resolution, and less susceptibility to the effects of Blood-Brain Barrier (BBB) permeability changes [7,30,32-34]. In addition, the current study adopted a new pCASL method based on the 3D-FSE sequence with spiral readout to increase SNR and reduce motion artefact and susceptibility distortion [35,36]. Due to the prominent labeling efficiency, superior SNR and lower inter-subject variability than conventional ASL, pCASL has become the best choice for brain perfusion and functional studies [7,37,38].

There were limitations in our research. First, CBF might be affected by chemotherapeutics, thus further research should take this into consideration. A further voxel-by-voxel analysis should be performed to acquire more accurate overall results.

This study suggests that early, transient, and complicated brain perfusion and GMV abnormalities caused by RT for NPC, which may be due to the micro-injuries of brain vascular and nerve tissues. No similar reports exist and therefore more research is required to confirm our results. Moreover, our research indicates that the new 3D FSE pCASL technique allows a complete exploration of global brain perfusion abnormalities induced by RT, and a more widely available clinical application in the future.

Conflict of Interest

The authors declare that there is no conflict of interest.

Acknowledgment

This work was supported by the Scientific Research Project of the Education Department of Hunan province (No: (2015) 54-15c1278) and the Scientific Research Project of the First People's Hospital of Chenzhou (N2014011) and National Science Foundation of China (Grant No. 81471251; 91649117; 81771344; 81560282 and 81360233).

References

1. Makale MT, McDonald CR, Hattangadi-Gluth JA, Kesari S. Mechanisms of radiotherapy-associated cognitive

- disability in patients with brain tumours. *Nat Rev Neurol* 2017; 13: 52-64.
2. Duan F, Cheng J, Jiang J, Chang J, Zhang Y, Qiu S. Whole-brain changes in white matter microstructure after radiotherapy for nasopharyngeal carcinoma: a diffusion tensor imaging study. *Eur Arch Otorhinolaryngol* 2016; 273: 4453-4459.
 3. Chen WS, Li JJ, Zhang JH, Hong L, Xing ZB, Wang F, Li CQ. Magnetic resonance spectroscopic imaging of brain injury after nasopharyngeal cancer radiation in early delayed reaction. *Genet Mol Res* 2014; 13: 6848-6854.
 4. Chen W, Qiu S, Li J, Hong L, Wang F, Xing Z, Li C. Diffusion tensor imaging study on radiation-induced brain injury in nasopharyngeal carcinoma during and after radiotherapy. *Tumori* 2015; 101: 487-490.
 5. Wang HZ, Qiu SJ, Lv XF, Wang YY, Liang Y, Xiong WF, Ouyang ZB. Diffusion tensor imaging and 1H-MRS study on radiation-induced brain injury after nasopharyngeal carcinoma radiotherapy. *Clin Radiol* 2012; 67: 340-345.
 6. Ghariq E, Teeuwisse WM, Webb AG, van Osch MJ. Feasibility of pseudocontinuous arterial spin labeling at 7 T with whole-brain coverage. *Magma* 2012; 25: 83-93.
 7. Borogovac A, Asllani I. Arterial Spin Labeling (ASL) fMRI: advantages, theoretical constraints, and experimental challenges in neurosciences. *Int J Biomed Imaging* 2012; 2012: 818456.
 8. Noguchi T, Kawashima M, Irie H, Ootsuka T, Nishihara M, Matsushima T, Kudo S. Arterial spin-labeling MR imaging in moyamoya disease compared with SPECT imaging. *Eur J Radiol* 2011; 80: 557-562.
 9. Wang C, Ding Y, Shen B, Gao D, An J, Peng K, Hou G, Zou L, Jiang M, Qiu S. Altered gray matter volume in stable chronic obstructive pulmonary disease with sub-clinical cognitive impairment: an exploratory study. *Neurotox Res* 2017; 31: 453-463.
 10. Ganzola R, Duchesne S. Voxel-based morphometry meta-analysis of gray and white matter finds significant areas of differences in bipolar patients from healthy controls. *Bipolar Disord* 2017; 19: 74-83.
 11. Kamagata K, Zalesky A, Hatano T, Ueda R, Di Biase MA, Okuzumi A, Shimoji K, Hori M, Caeyenberghs K, Pantelis C, Hattori N, Aoki S. Gray matter abnormalities in idiopathic Parkinson's Disease: Evaluation by diffusional kurtosis imaging and neurite orientation dispersion and density imaging. *Hum Brain Mapp* 2017.
 12. van der Lee SJ, Roshchupkin GV, Adams HH, Schmidt H, Hofer E, Saba Y, Schmidt R, Hofman A, Amin N, van Duijn CM, Vernooij MW, Ikram MA, Niessen WJ. Gray matter heritability in family-based and population-based studies using voxel-based morphometry. *Hum Brain Mapp* 2017; 38: 2408-2423.
 13. Song XW, Dong ZY, Long XY, Li SF, Zuo XN, Zhu CZ, He Y, Yan CG, Zang YF. REST: a toolkit for resting-state functional magnetic resonance imaging data processing. *PLoS One* 2011; 6: e25031.
 14. Yan CG, Wang XD, Zuo XN, Zang YF. DPABI: Data Processing and Analysis for (Resting-State) Brain Imaging. *Neuroinformatics* 2016; 14: 339-351.
 15. Tan XP, Zhao JQ, Liang BL, Xie BK, Zhong JL, Ye RX. Diagnostic value of MR diffusion tensor imaging on radiation-induced early brain injury of nasopharyngeal carcinoma after radiotherapy. *Ai Zheng* 2004; 23: 1334-1337.
 16. Xiong WF, Qiu SJ, Wang HZ, Lv XF. 1H-MR spectroscopy and diffusion tensor imaging of normal-appearing temporal white matter in patients with nasopharyngeal carcinoma after irradiation: initial experience. *J Magn Reson Imaging* 2013; 37: 101-108.
 17. Vitorino R, Hojjat SP, Cantrell CG, Feinstein A, Zhang L, Lee L, O'Connor P, Carroll TJ, Aviv RI. Regional frontal perfusion deficits in relapsing-remitting multiple sclerosis with cognitive decline. *AJNR Am J Neuroradiol* 2016.
 18. D'haeseleer M, Hostenbach S, Peeters I, Sankari SE, Nagels G, De Keyser J, D'hooghe MB. Cerebral hypoperfusion: a new pathophysiologic concept in multiple sclerosis? *J Cereb Blood Flow Metab* 2015; 35: 1406-1410.
 19. Torihata H, Ishikawa F, Okada Y, Tanaka Y, Uchida T, Suguro T, Kakiuchi T. Irradiation up-regulates CD80 expression through two different mechanisms in spleen B cells, B lymphoma cells, and dendritic cells. *Immunology* 2004; 112: 219-227.
 20. Wu KL, Tu B, Li YQ, Wong CS. Role of intercellular adhesion molecule-1 in radiation-induced brain injury. *Int J Radiat Oncol Biol Phys* 2010; 76: 220-228.
 21. Liu Y, Xiao S, Liu J, Zhou H, Liu Z, Xin Y, Suo WZ. An experimental study of acute radiation-induced cognitive dysfunction in a young rat model. *AJNR Am J Neuroradiol* 2010; 31: 383-387.
 22. Rakic P. Neurogenesis in adult primate neocortex: an evaluation of the evidence. *Nat Rev Neurosci* 2002; 3: 65-71.
 23. Fischl B, van der Kouwe A, Destrieux C, Halgren E, Ségonne F, Salat DH, Busa E, Seidman LJ, Goldstein J, Kennedy D, Caviness V, Makris N, Rosen B, Dale AM. Automatically parcellating the human cerebral cortex. *Cereb Cortex* 2004; 14: 11-22.
 24. Alosco ML, Gunstad J, Xu X, Clark US, Labbe DR, Riskin-Jones HH, Terrero G, Schwarz NF, Walsh EG, Poppas A, Cohen RA, Sweet LH. The impact of hypertension on cerebral perfusion and cortical thickness in older adults. *J Am Soc Hypertens* 2014; 8: 561-570.
 25. Brunet E, Sarfati Y, Hardy-Baylé MC, Decety J. Abnormalities of brain function during a non-verbal theory of mind task in schizophrenia. *Neuropsychologia* 2003; 41: 1574-1582.
 26. Dieterich M, Bartenstein P, Spiegel S, Bense S, Schwaiger M, Brandt T. Thalamic infarctions cause side-specific suppression of vestibular cortex activations. *Brain* 2005; 128: 2052-2067.

Use of 3D-ASL and VBM to analyze abnormal changes in brain perfusion and gray areas in nasopharyngeal carcinoma patients undergoing radiotherapy

27. Wang J, Aguirre GK, Kimberg DY, Roc AC, Li L, Detre JA. Arterial spin labeling perfusion fMRI with very low task frequency. *Magn Reson Med* 2003; 49: 796-802.
28. Detre JA, Rao H, Wang DJ, Chen YF, Wang Z. Applications of arterial spin labeled MRI in the brain. *J Magn Reson Imaging* 2012; 35: 1026-1037.
29. Chen Y, Wolk DA, Reddin JS, Korczykowski M, Martinez PM, Musiek ES, Newberg AB, Julin P, Arnold SE, Greenberg JH, Detre JA. Voxel-level comparison of arterial spin-labeled perfusion MRI and FDG-PET in Alzheimer disease. *Neurol* 2011; 77: 1977-1985.
30. Lehmann P, Monet P, de Marco G, Saliou G, Perrin M, Stoquart-Elsankari S, Bruniau A, Vallée JN. A comparative study of perfusion measurement in brain tumours at 3 Tesla MR: Arterial spinlabeling versus dynamic susceptibility contrast-enhanced MRI. *Eur Neurol* 2010; 64: 21-26.
31. Zou Q, Wu CW, Stein EA, Zang Y, Yang Y. Static and dynamic characteristics of cerebral blood flow during the resting state. *Neuroimage* 2009; 48: 515-524.
32. Alsop DC, Detre JA, Grossman M. Assessment of cerebral blood flow in Alzheimer's disease by spin-labeled magnetic resonance imaging. *Ann Neurol* 2000; 47: 93-100.
33. Zaharchuk G, El Mogy IS, Fischbein NJ, Albers GW. Comparison of arterial spin labeling and bolus perfusion-weighted imaging for detecting mismatch in acute stroke. *Stroke* 2012; 43: 1843-1848.
34. Wang DJ, Alger JR, Qiao JX, Hao Q, Hou S, Fiaz R, Gunther M, Pope WB, Saver JL, Salamon N, Liebeskind DS. UCLA Stroke Investigators. The value of arterial spin-labeled perfusion imaging in acute ischemic stroke: comparison with dynamic susceptibility contrast-enhanced MRI. *Stroke* 2012; 43: 1018-1024.
35. Ding B, Ling HW, Zhang Y, Huang J, Zhang H, Wang T, Yan FH. Pattern of cerebral hyperperfusion in Alzheimer's disease and amnesic mild cognitive impairment using voxel-based analysis of 3D arterial spin-labeling imaging: initial experience. *Clin Interv Aging* 2014; 9: 493-500.
36. Chen TY, Chiu L, Wu TC, Wu TC, Lin CJ, Wu SC, Tsui YK. Arterial spin-labeling in routine clinical practice: a preliminary experience of 200 cases and correlation with MRI and clinical findings. *Clin Imaging* 2012; 36: 345-352.
37. Dai W, Garcia D, de Bazelaire C, Alsop DC. Continuous flow-driven inversion for arterial spin labeling using pulsed radio frequency and gradient fields. *Magn Reson Med* 2008; 60: 1488-1497.
38. Gevers S, van Osch MJ, Bokkers RP, Kies DA, Teeuwisse WM, Majoie CB, Hendrikse J, Nederveen AJ. Intra- and multicenter reproducibility of pulsed, continuous and pseudo-continuous arterial spinlabeling methods for measuring cerebral perfusion. *J Cereb Blood Flow Metab* 2011; 31: 1706-1715.

***Correspondence to**

Shijun Qiu
Department of Medical Imaging Center
Nanfang Hospital
Southern Medical University
Guangzhou
PR China